



HAL
open science

Atmospheric Interface Reentry Point Targeting Using Aerodynamic Drag Control

Josep Virgili, Peter C E Roberts, Nathan C Hara

► **To cite this version:**

Josep Virgili, Peter C E Roberts, Nathan C Hara. Atmospheric Interface Reentry Point Targeting Using Aerodynamic Drag Control. *Journal of Guidance, Control, and Dynamics*, 2015, 38, pp.403 - 413. 10.2514/1.g000884 . hal-04225677

HAL Id: hal-04225677

<https://hal.science/hal-04225677>

Submitted on 3 Oct 2023

HAL is a multi-disciplinary open access archive for the deposit and dissemination of scientific research documents, whether they are published or not. The documents may come from teaching and research institutions in France or abroad, or from public or private research centers.

L'archive ouverte pluridisciplinaire **HAL**, est destinée au dépôt et à la diffusion de documents scientifiques de niveau recherche, publiés ou non, émanant des établissements d'enseignement et de recherche français ou étrangers, des laboratoires publics ou privés.

Atmospheric Interface Reentry Point Targeting Using Aerodynamic Drag Control

Josep Virgili,^{*} Peter C. E. Roberts,[†] and Nathan C. Hara[‡]
Cranfield University, Cranfield, England MK43 0AL, United Kingdom

The ability to control the location of a spacecraft atmospheric interface reentry has been traditionally accomplished using propulsion. A novel technique is presented here where a predefined point of atmospheric interface reentry is achieved by adjusting the aerodynamic drag of a spacecraft in a circular orbit. If this method is employed at a sufficiently high starting altitude, any ground-track point accessible by the orbit can be targeted. This method can be broken up into two different parts. The first consists of finding the decay profile that achieves the desired reentry location. The second consists of keeping the spacecraft within this nominal decay trajectory, given the atmospheric uncertainty and other perturbations. The two parts of this method are presented here in detail. Finally, a case study is provided to demonstrate how this method could work in a realistic scenario and to evaluate its performance. The case study shows that a reentry point can be targeted with a 3σ error of less than 200 km, using a typical Global Positioning System for navigation. Finally, a discussion of potential applications is provided.

Nomenclature

A_{ref}	=	spacecraft's reference area, m^2
a	=	semimajor axis, m
a_D	=	acceleration due to drag, m/s^2
C_B	=	ballistic coefficient, m^2/kg
C_D	=	drag coefficient
H	=	atmospheric scale height, m
h	=	altitude, m
i	=	orbit inclination, rad
J_2	=	Earth's oblateness coefficient
m	=	spacecraft mass, kg
n	=	mean motion, rad/s
q	=	dynamic pressure, N/m^2
t	=	time, s
u	=	argument of latitude, rad
V	=	relative velocity of the flow, m/s
\mathbf{x}	=	state vector
λ	=	longitude, rad
μ	=	gravitational constant of the Earth, m^3/s^2
ρ	=	atmospheric density, kg/m^3
Φ	=	state transition function
ϕ	=	latitude, rad
Ω	=	right ascension of the ascending node, rad

I. Introduction

THE aerodynamic forces experienced by spacecraft orbiting in low Earth orbit are usually considered perturbations that need to be avoided or compensated. Although this is generally the case, these aerodynamic forces can be controlled and exploited to achieve a useful purpose. Research has already been conducted to use aerodynamic drag to perform an aerocapture, control a spacecraft orbit, rendezvous with another vehicle, do formation flight, and do constellation maintenance [1–8]. Also, the use of aerodynamic forces has also been studied to control the attitude of a spacecraft [9–11].

Received 7 July 2014; revision received 12 October 2014; accepted for publication 13 October 2014; published online 28 January 2015. Copyright © 2014 by the American Institute of Aeronautics and Astronautics, Inc. All rights reserved. Copies of this paper may be made for personal or internal use, on condition that the copier pay the \$10.00 per-copy fee to the Copyright Clearance Center, Inc., 222 Rosewood Drive, Danvers, MA 01923; include the code 1533-3884/15 and \$10.00 in correspondence with the CCC.

^{*}Researcher, Space Research Centre; j.virgilillop@cranfield.ac.uk.

[†]Lecturer, Space Research Centre; currently Lecturer, University of Manchester, Manchester, England M13 9PL, United Kingdom; p.c.e.roberts@cranfield.ac.uk.

[‡]Postgraduate Student, Space Research Centre; n.c.hara@cranfield.ac.uk.

Here a novel method is presented where the aerodynamic drag is used to target the atmospheric interface reentry point of a spacecraft's decaying orbit. The method presented here has been only applied to circular orbits and its extension to eccentric orbits is left for future studies. The assumption of circular orbits is not only applied to the initial orbit, but is also enforced as the orbit decays. It is also important to note that the method presented here only controls the location of the atmospheric interface reentry point and not the landing or impact point (if the spacecraft was to survive reentry). The atmospheric interface reentry point, also known as the entry interface in the literature, can be defined as the point where the interaction of the spacecraft with the atmosphere is so great, in terms of aerodynamic forces, that these forces completely dominate the flight dynamics. The altitude when this occurs depends on the vehicle aerodynamic properties and the atmospheric conditions, but it is usually set between 120–90 km [12]. Here an intermediate altitude of 100 km has been selected.

The control of the aerodynamic drag is assumed to be achieved through the control over the ballistic coefficient. Therefore, the drag is modulated to achieve the desired decay rate at all times. How to control the ballistic coefficient of a spacecraft and its practical considerations are outside the scope of this paper, but it is not difficult to envision simple ways to do so. For example, changing the cross-sectional area of the spacecraft by changing the attitude of the spacecraft or by altering the geometry of a drag sail would do.

Changing the ballistic coefficient, by changing the cross-sectional area, for example, is enough to alter the drag that the spacecraft creates, but it is not enough to have knowledge of this drag. The knowledge of the atmospheric properties (mainly density) is required to bridge the gap between controlling the ballistic coefficient and controlling the drag. This information of the atmospheric conditions can be obtained by using atmospheric models (estimation) or by using in situ measurements by onboard sensors. A detailed analysis of how to obtain this information has also been left outside the scope of this paper.

The idea of using drag to control certain parameters of the atmospheric interface reentry location is not completely new. Some work has been done to use a sudden drag increase in the last few hours of the decay to reduce the uncertainty of the time and location of the reentry interface [13]. The same approach is taken in [14] where a sudden increase in drag in the last few orbits is used to make the spacecraft reenter over an unpopulated area and reduce the risk to population and property that any surviving parts that reach the ground might pose. These two works, using the same method, only provide a limited capability to change the atmospheric interface reentry location in the along-track direction. Because this is done close to the reentry interface, the accessible targets are limited to the locations defined (approximately) by the last few orbits' ground track (along track). The method presented here starts modulating the drag at much

higher altitudes and has cross-track targeting capabilities. The combination of along- and cross-track targeting capabilities gives more freedom to select the target and can also be used to achieve global coverage (latitude limited only by the orbit's inclination).

Research has also been conducted in using drag modulation to achieve more precise landings and aerocaptures on Mars [3,15]. Drag modulation can also be used during the atmospheric reentry to reduce the aerodynamic loads [16] and to simplify the control during the descent [17]. The general drag modulation effects on flight dynamics was first studied by Rose and Hayes in 1963 [18].

The method presented in this paper is an orbit-control technique that aims to control the spacecraft's decay (before reentry) such that the spacecraft reenters over a predefined location. Such a method could prove useful for drag-enhancing deorbit devices deorbiting large spacecraft, where some components of the spacecraft are expected to survive reentry. In this case, this technique could be used to avoid reentering over populated areas. This would be used as a risk-reduction strategy compared with uncontrolled decays. Also, this method could be applied to provide a passive method for small reentry capsules to crudely target their landing area. When targeting the atmospheric interface reentry location, the landing area of the surviving capsule would be limited, although potentially still quite large. If the capsule has a way to control its trajectory during its atmospheric reentry, the landing area could be reduced.

The method presented here is an alternative to the traditional approach of targeting the atmospheric interface reentry location by a sudden orbit change caused by an impulsive burn (deorbit burn) [19,20]. This traditional approach has been used to deorbit spacecraft so that they burn up in the atmosphere (to avoid debris buildup or to avoid uncontrolled reentries) and has also been used in vehicles that survive reentry and land or impact in a predefined location. The method presented here could provide some advantages over the traditional approach on some specific scenarios.

During the atmospheric phase of the reentry, if the vehicle is capable of surviving it, the trajectory can also be controlled using aerodynamic forces. This is a discipline on its own [12,21]. The control of the trajectory during atmospheric flight phase is outside of the scope of this paper.

II. Problem Statement

The problem consists of making a spacecraft reentry interface occur over a predesignated ground point by changing its ballistic coefficient. The problem can be considered solved when a time history of the ballistic coefficient that makes the spacecraft satisfy the previous condition is provided.

To find an appropriate solution, the problem can be subdivided into two independent problems that can be tackled independently:

1) Compute a nominal trajectory that would make the spacecraft reenter over the designated point. To compute the nominal trajectory, it is assumed that the atmospheric environment is well known and that the spacecraft ballistic coefficient can be perfectly controlled. This step essentially delivers the nominal ballistic coefficient time history that the spacecraft needs to follow.

2) Implement a control algorithm to make the spacecraft follow the nominal trajectory in the presence of the variations in the atmospheric environment and the uncertainties of the ballistic coefficient.

It is important to reiterate that here the point that is targeted is the atmospheric interface reentry point and not the impact/landing point. This is an important difference. Because it is difficult to define where the reentry starts, it is assumed that it starts when the spacecraft decays below 100 km [12]. Although this definition is somewhat arbitrary and the 100 km altitude will need to be adjusted depending on each case, it does not change the approach or the methodology presented here. A small change in this altitude has also a negligible impact on the accuracy of the method.

III. Nominal Trajectory

If a spacecraft maintains a constant ballistic coefficient C_B during all its decay, it will reenter over a certain point. This reentry interface

point is a function of the spacecraft's initial position and velocity, its ballistic coefficient, the Earth's gravity field, the atmospheric environment, and other forces (such as solar radiation pressure and third-body perturbations). If one of the mentioned parameters changes, then the reentry interface location will also change. Therefore, assuming everything else remains constant, a simple method to change the reentry interface location would be to change the spacecraft ballistic coefficient to a different constant value. If this is the case, and the spacecraft can adopt a range of different ballistic coefficients that are to be maintained constant throughout its decay, then the spacecraft can alter its reentry interface location, but only along a line. Figure 1 shows how the reentry interface location moves as the constant ballistic coefficient used during the decay changes. The figure has been produced considering an initial 70 deg inclination circular orbit, decaying from 300 to 100 km altitude and with ballistic coefficients ranging from $C_{B1} = 0.021$ to $C_{B2} = 0.0200$ m²/kg. The line shown in Fig. 1 is the reentry interface point locus, and it closely resembles the orbit ground track but is not the same.

The simple strategy to change the spacecraft ballistic coefficient to a different constant value can be useful at the final stages of the decay because it allows one to target a point along the reentry point locus (only along track). This approach has been used in previous works [13,14]. However, this simple strategy is not very useful if global coverage is required, because it does not provide any cross-track targeting capabilities. This strategy, of changing the ballistic coefficient that is maintained constant during the decay, essentially targets the argument of latitude of the reentry, and the time of reentry is a by product of targeting the argument of latitude. Therefore, the position of the spacecraft in the orbit plane when it reenters is specified by the target argument of latitude, and the by product time of reentry fixes the position of the Earth with respect to the orbit plane. So, the argument of latitude fixes the latitude of the reentry point and the time of reentry fixes its longitude. To get cross-track capabilities, these two variables (time of reentry and argument of latitude at reentry) need to be controlled independently.

Targeting the reentry time independently from the argument of latitude can be achieved by changing the ballistic coefficient during the orbital decay $C_B = f(t)$. Having a time-varying ballistic coefficient during the decay can be used to achieve different decay profiles. Figure 2a shows the evolution of the altitude with respect to the orbit count (argument of latitude), and Fig. 2b shows it with respect to time, for three different ballistic coefficient profile scenarios that share the same initial conditions and atmosphere. These figures show that different ballistic coefficient profiles can make the spacecraft reenter at the same argument of latitude (and hence at the same latitude) but at different times (and hence at different longitudes). The reentry time of these three trajectories can be computed by adding the period of all their orbits and, because their decay profiles are different, their reentry time will be different (hence reentering at different longitudes).

The three example trajectories shown in Fig. 2a can be classified looking at their relative decay rates. The trajectory with a constant ballistic coefficient throughout the decay $C_B = k$ will serve as a reference. Then, $C_B = f_1(t)$ shows a slower decay at the beginning

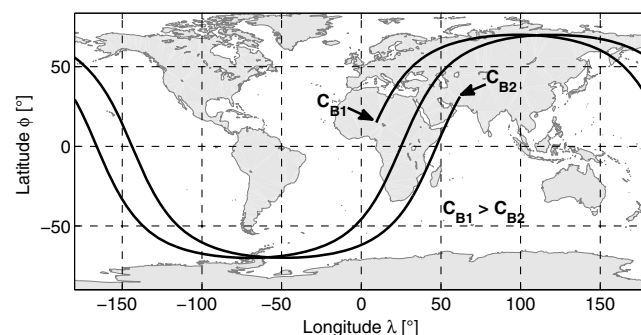


Fig. 1 Atmospheric interface reentry points (not to be confused with a ground track) applying different constant ballistic coefficients C_B throughout the decay.

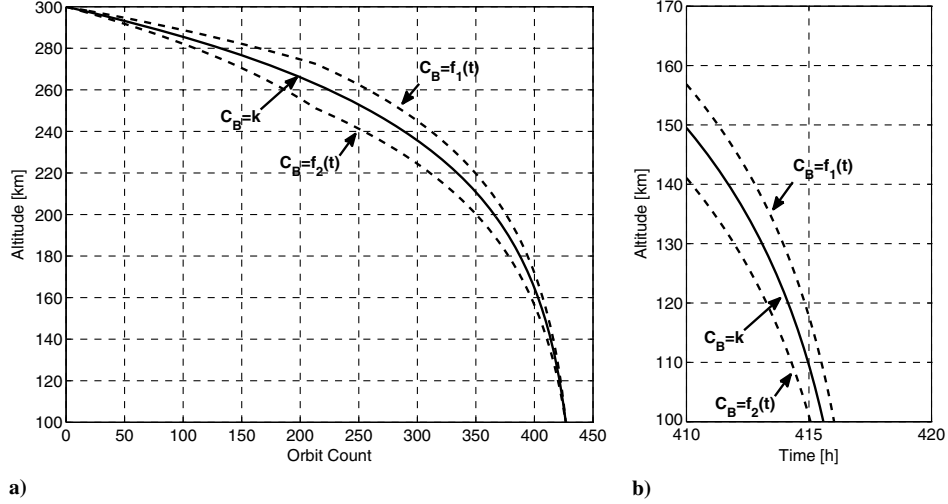


Fig. 2 Altitude decay a) with respect to orbit count (proportional to argument of latitude) and b) detail of last part of decay.

and a more rapid decay at the end (slow-rapid) and $C_B = f_2(t)$ shows a more rapid decay at the beginning and a slower decay at the end (rapid-slow) when compared with the reference decay $C_B = k$. Therefore, the trajectory with a slow-rapid decay will spend more orbits at a higher altitude (where the orbital period is longer) than the reference trajectory ($C_B = k$), and hence it will reenter at the same argument of latitude (same latitude) but at a later time (westward longitude). Also, the trajectory with a rapid-slow decay spends more orbits at a lower altitude (where the period is shorter) than the reference trajectory ($C_B = k$), and hence it will reenter at the same argument of latitude (same latitude) but at an earlier time (eastward longitude). This technique to target independently the reentry time and the reentry argument of latitude can be exploited to target the reentry point latitude and longitude, thus achieving cross-track targeting capabilities.

A convenient way to explore the dynamics of such a method is to discretize the ballistic coefficient function so that the whole time interval is composed of segments of constant ballistic coefficient. Figure 3 shows the trajectory broken down into these discrete segments. In this scenario, a state transition function can be defined as in Eq. (1) so that it outputs the next state vector \mathbf{x}_{n+1} from the current state vector \mathbf{x}_n , assuming that the ballistic coefficient remains constant in that interval. As is defined in Eq. (1), this state transition function outputs the difference between two consecutive state vectors so that, if the current state vector is known \mathbf{x}_n , the next state vector \mathbf{x}_{n+1} can be then computed:

$$\mathbf{x}_{n+1} = \Phi_n(\mathbf{x}_n, C_B) + \mathbf{x}_n \quad (1)$$

If this state transition function could be computed, the effects of an arbitrary ballistic coefficient time function could be evaluated. The construction of such functions can be done using numerical propagators, but their results lack the insight provided by an analytical approach. If the dynamics of the problem are sufficiently simplified, analytical expressions of this state transition function can be found, therefore providing an insight into the dynamics of the problem. With the analytical expressions, solutions can be easily found. These solutions can then be used as first guesses in the numerical algorithms.

In the sections that follow, a method to construct the nominal trajectory is provided. First, to provide an insight into the problem, the nominal trajectory will be constructed analytically (using simplified dynamic models) and then some comments will be made when using numerical propagators (with accurate dynamic models).

A. Analytical Approach Using Simplified Dynamic Models

The main simplifications that will be assumed are that there will be only two forces shaping the orbit. First, the gravitational pull of the Earth is modeled as a point mass with the contribution due to the Earth's oblateness J_2 . The second force considered is the aerodynamic drag caused by the interaction of the spacecraft with an exponential atmosphere. Under these assumptions, the orbit of a spacecraft can be considered Keplerian but with secular variations on its orbital parameters. Also, the physical body of the Earth will be modeled as a sphere with a radius of R_\oplus , and finally, it will be assumed that the orbits are circular throughout the decay. Under these assumptions, a good representation of the state vector can be the orbital parameters describing a circular orbit:

$$\mathbf{x} = [t, u, a, \Omega, i] \quad (2)$$

where t refers to the time, a is the semimajor axis, u is the argument of latitude, Ω is the right ascension of the ascending node (RAAN), and i is the orbit's inclination. At this point, it is pertinent to explicitly state that, under the current assumptions, the orbit's altitude h can be related to the orbit's semimajor axis a by $h = a - R_\oplus$, and so their role as state vector variables is interchangeable. Here, the semimajor axis is used, but the altitude will appear in the figures to make their interpretation easier.

The general effect of drag is to make orbits decay and to circularize them [22]. Therefore, if the initial orbit is circular, it will remain circular during the entire decay. The only way for an orbit that is initially circular and that decays due to aerodynamic drag to become eccentric is if the drag force was variable in the short term and its

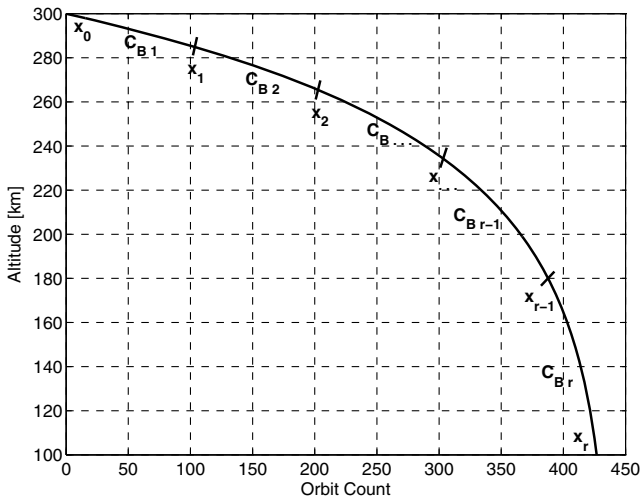


Fig. 3 Discretization of the ballistic coefficient function.

frequency would make it resonate with the orbital period. For example, if a significantly larger drag was experienced always at the same true anomaly, then the orbit would become eccentric with this particular true anomaly becoming the apogee. Because this method does not attempt to create such resonances, it can be safely assumed that the orbit remains quasi circular during the entire decay.

1. State Transition Function

In a decaying orbit, the state vector parameters will change during the decay. The objective of this section is to obtain a function that can interrelate the state variable changes during the decay to one of the state variables that will serve as a reference. This function is the state transition function.

Here, all the state variables will be written in terms of the semimajor axis as $t, u, \Omega, i = f(a)$. Therefore, the discretization shown in Fig. 3 will be defined by the semimajor axis at the segment limits.

The process to obtain the state transition function can start with the inclination, the simplest case, because an orbit subject to aerodynamic drag will decay with a constant inclination. This assumption holds when only J_2 and aerodynamic drag effects from a stationary atmosphere are considered [22] (these are the assumptions made). Therefore, i is a constant during the decay and hence is not a function of a . This can be easily written as

$$i_{n+1} = i_n = i_0 \quad (3)$$

The only secular change in the semimajor axis will be produced by the aerodynamic drag (J_2 produces only a periodic change). The time elapsed with respect to a semimajor axis change when subject to aerodynamic drag in a circular orbit can be written as in Eq. (4), extracted from [23] (already simplified for circular orbits):

$$\frac{dt}{da} = -\frac{n}{2a_D} \quad (4)$$

where a_D is the acceleration due to drag, and $n = \sqrt{\mu/a^3}$ is the mean motion, with μ being the gravitational constant of the Earth. Then, the acceleration due to drag can be written as

$$a_D = qC_B \quad (5)$$

$$q = \frac{1}{2}\rho V^2 \quad (6)$$

where q is the dynamic pressure that is a function of the atmospheric density ρ and the relative velocity of the spacecraft with respect to the flow V . Although the atmosphere corotates with the Earth [24] and there are atmospheric winds [25], here a stationary atmosphere has been assumed, and hence V can be assumed as the spacecraft orbital velocity. The ballistic coefficient C_B is defined in Eq. (7) and is a function of the spacecraft's reference area A_{ref} , its drag coefficient C_D , and its mass m [26]:

$$C_B = \frac{A_{\text{ref}}C_D}{m} \quad (7)$$

By grouping all the constant terms in Eq. (5) in the constant $K_1 = C_B/2$, the drag acceleration expression can be simplified as follows:

$$a_D = K_1\rho V^2 \quad (8)$$

As already mentioned in the assumptions, the density will be modeled according to an exponential atmosphere, thus

$$\rho(a) = \rho_0 \exp\left[-\frac{a - a_0}{H}\right] \quad (9)$$

where ρ_0 is the density at semimajor axis a_0 , and where H represents the scale height. Also, if we assume that the velocity relative to the flow is the orbital velocity and apply the assumption that the orbit will be quasi circular throughout the decay, then

$$V = \sqrt{\frac{\mu}{a}} \quad (10)$$

Combining Eq. (8) with Eqs. (9) and (10), the change in the semimajor axis can be rewritten as

$$\frac{dt}{da} = \frac{1}{K_2\sqrt{a}e^{-a/H}} + c_1 \quad (11)$$

where K_2 is a compact representation of the constant terms:

$$K_2 = -2K_1\sqrt{\mu}\rho_0e^{a_0/H} = -C_B\sqrt{\mu}\rho_0e^{a_0/H} \quad (12)$$

Making use of the following variable time transformation $t = u/n$, then Eq. (11) can be written in terms of argument of latitude. Multiplying Eq. (11) by $n = du/dt$ yields

$$\frac{du}{da} = \frac{1}{K_3a^2e^{-a/H}} + c_2 \quad (13)$$

again, with the constant terms included in K_3 :

$$K_3 = \frac{K_2}{\sqrt{\mu}} = -C_B\rho_0e^{a_0/H} \quad (14)$$

Integrating Eq. (11) results in (where erfi is the imaginary error function)

$$f_i(a) = \int \frac{1}{K_2\sqrt{a}e^{-a/H}} da = \frac{\sqrt{\pi}\sqrt{H}\text{erfi}(\sqrt{a/H})}{K_2} + c_1 \quad (15)$$

Integrating Eq. (13) results in (where Ei is the exponential integral)

$$f_u(a) = \int \frac{1}{K_3a^2e^{-a/H}} da = \frac{a\text{Ei}(a/H) - He^{a/H}}{K_3Ha} + c_2 \quad (16)$$

The c_1 and c_2 terms in Eqs. (15) and (16) are constants resulting from the integration process of the indefinite integrals. A similar expression for RAAN Ω can be obtained by looking at the change in RAAN produced by the Earth's oblateness [23]:

$$\frac{d\Omega}{dt} = -\frac{3nR_{\oplus}^2J_2}{2a^2}\cos i = K_4a^{-7/2} \quad (17)$$

$$K_4 = -\frac{3R_{\oplus}^2J_2\cos i\sqrt{\mu}}{2} \quad (18)$$

This expression can be written, in terms of $d\Omega/da$, if it is combined with Eq. (11) as

$$\frac{d\Omega}{da} = K_5a^{-4}e^{a/H} \quad (19)$$

$$K_5 = \frac{K_4}{K_2} = \frac{3R_{\oplus}^2J_2\cos i}{2C_B\rho_0e^{a_0/H}} \quad (20)$$

Integrating Eq. (19) results in (with c_3 being a constant)

$$f_{\Omega}(a) = \int K_5 a^{-4} e^{a/H} da$$

$$= \frac{K_5 [a^3 \text{Ei}(a/H) - H e^{a/H} (2H^2 + Ha + a^2)]}{6H^3 a^3} + c_3 \quad (21)$$

Then, functions f_t , f_u , and f_{Ω} can be used to compute the state vector at any semimajor axis (altitude) during a decay, provided that the ballistic coefficient remains constant. These functions can also be used then to compute the state vector at the different segment limits as follows:

$$t_n - t_{n-1} = \Delta t_n = f_t(a_n, C_{Bn}) - f_t(a_{n-1}, C_{Bn}) \quad (22)$$

$$u_n - u_{n-1} = \Delta u_n = f_u(a_n, C_{Bn}) - f_u(a_{n-1}, C_{Bn}) \quad (23)$$

$$\Omega_n - \Omega_{n-1} = \Delta \Omega_n = f_{\Omega}(a_n, C_{Bn}) - f_{\Omega}(a_{n-1}, C_{Bn}) \quad (24)$$

$$i_{n+1} - i_n = \Delta i_n = 0 \quad (25)$$

The state transition function can then be written as

$$\Phi_n = \begin{bmatrix} f_t(a_n, C_{Bn}) - f_t(a_{n-1}, C_{Bn}) \\ f_u(a_n, C_{Bn}) - f_u(a_{n-1}, C_{Bn}) \\ a_n - a_{n-1} \\ f_{\Omega}(a_n, C_{Bn}) - f_{\Omega}(a_{n-1}, C_{Bn}) \\ 0 \end{bmatrix} \quad (26)$$

Therefore, if an initial set of conditions are set \mathbf{x}_0 , all the subsequent state vectors up until reentry $\mathbf{x}_0, \mathbf{x}_1, \dots, \mathbf{x}_n, \dots, \mathbf{x}_{r-1}, \mathbf{x}_r$ can be computed using the formulas provided in this section. This can be written in a function format as follows:

$$\mathbf{x}_n = \begin{bmatrix} t_n \\ u_n \\ a_n \\ \Omega_n \end{bmatrix} = [\mathbf{x}_0 + \Phi_1 + \dots + \Phi_n] = F_{xn} \left(\begin{array}{c} \mathbf{x}_0 \\ a_0, \dots, a_n \\ C_{B1}, \dots, C_{Bn} \end{array} \right) \quad (27)$$

This last function F_{xn} can be used to compute the state vector at any semimajor axis (altitude) during a decay, providing that the ballistic coefficient can be discretized as a function of the semimajor axis.

2. Latitude and Longitude

The state vector is useful but it does not explicitly provide the latitude ϕ and longitude λ where the spacecraft is located over the Earth. The latitude can be computed using spherical trigonometry with the following formula:

$$\sin \phi = \sin u \sin i \quad (28)$$

The longitude can be computed as follows:

$$\lambda = \lambda_{AN0} + (\Omega - \Omega_0) + \arcsin(\tan \phi \sin i) - \omega_{\oplus} t \quad (29)$$

where λ_{AN0} is the initial longitude of the ascending node, Ω_0 is the initial RAAN, and ω_{\oplus} is the Earth's angular velocity. The latitude and longitude can be related to the orbit state vector (although some of the state variables are not directly relevant to compute ϕ and λ) through the following function:

$$\begin{bmatrix} \phi \\ \lambda \end{bmatrix} = \begin{bmatrix} \arcsin(\sin u \sin i) \\ \lambda_0 + (\Omega - \Omega_0) + \arcsin(\tan \phi \sin i) - \omega_{\oplus} t \end{bmatrix}$$

$$= F_{\phi,\lambda}(t, u, a, \Omega, i) \quad (30)$$

Therefore, the function G_n defined in Eq. (31) can be used to compute the latitude and longitude at any semimajor axis (altitude) during a decay, providing that the ballistic coefficient can be discretized as a function of the semimajor axis:

$$G_n = F_{\phi,\lambda}(F_{xn}) \quad (31)$$

3. Strategy

It is clear that, to adjust the latitude and the longitude, only two degrees of freedom are required. The strategy envisioned by the authors assumes that the spacecraft can alter its ballistic coefficient within a range $[C_{B \min}, C_{B \max}]$ where a mean or nominal ballistic coefficient can be defined as $C_{B \text{mean}} = (C_{B \max} + C_{B \min})/2$. To provide enough degrees of freedom, the spacecraft will maintain an initial ballistic coefficient C_{B1} from its initial altitude a_0 until it reaches a transition altitude a_t where it will transition to a second ballistic coefficient C_{B2} , which will be maintained until reentry a_r . Assuming that the initial position cannot be chosen and that the reentry altitude is fixed, this approach seems to have three degrees of freedom (C_{B1} , C_{B2} , and a_t). To reduce this to the only two degrees of freedom required, it will be assumed that both ballistic coefficients are equidistant to the mean ballistic coefficient, but with one being higher and the other being lower ($C_{B1} = C_{B \text{mean}} + \Delta C_B$ and $C_{B2} = C_{B \text{mean}} - \Delta C_B$). Note that ΔC_B can be either positive or negative and that, for this strategy to be successful, C_{B1} and C_{B2} need to be within the achievable range (and potentially leave some control authority for the onboard trajectory control). With this strategy, the parameters are reduced to the transition altitude a_t and the ballistic coefficient delta ΔC_B . This arrangement is schematically shown in Fig. 4.

Note that some margin of the $[C_{B \min}, C_{B \max}]$ range is left for the onboard control, ensuring that the spacecraft can maintain the required decay rate in the presence of uncertainty (mainly in the atmospheric density, which is highly variable and difficult to forecast). The amount of margin that needs to be left depends on several parameters and needs to be evaluated on a case-by-case basis. Section IV covers how to control the decay (using the available margin).

Then, a way to explore the area that can be targeted is to set ΔC_B to its maximum (so that the ballistic coefficients reach their maximum and minimum) and move the transition semimajor axis a_t from a_0 to a_r . This process will produce two lines (one for positive ΔC_B and another one with negative ΔC_B) that separately will resemble the one shown in Fig. 1 and that, when plotted together, will enclose the area that the spacecraft is capable to target. An exaggerated example of this is shown in Fig. 5. The values used to produce this figure are

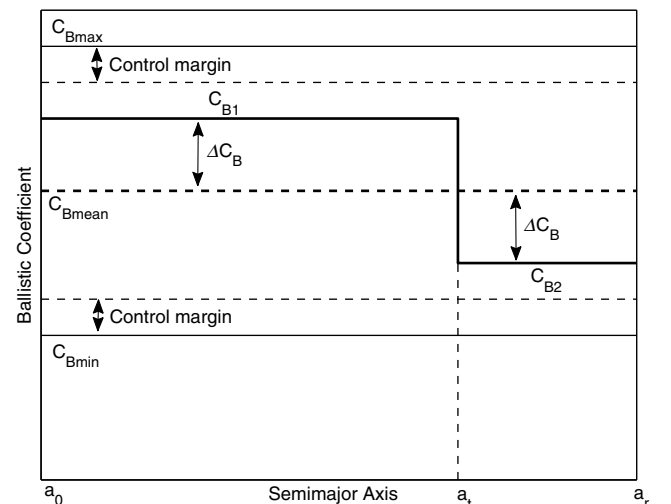


Fig. 4 Outline of the proposed control strategy.

$h_0 = 200$ km, $h_f = 100$ km, $C_{B \max} = 0.0223$ m²/kg, $C_{B \min} = 0.0222$ m²/kg, $i = 70$ deg, $H = 55$ km, $\rho_0 = 6.66 \times 10^{-12}$ kg/m³, and $a_{\rho_0} = 350$ km, with the longitude difference between the two lines being exaggerated by a factor of 750. The centerline in Fig. 5 can be obtained by setting a constant ballistic coefficient throughout the decay and then scanning through all possible ballistic coefficients.

Note that the difference between $C_{B \max}$ and $C_{B \min}$ used in Fig. 5 is very small. This small difference ensures that the points of reentry, when using a constant $C_{B \max}$ or $C_{B \min}$, are sufficiently close to each other so that Fig. 5 is clear (no lines crossing each other as in Fig. 1). Because of this small difference, the accessible area is also very small and it has to be exaggerated to make visible in Fig. 5. When this method is used in a real case, the difference between $C_{B \max}$ and $C_{B \min}$ should be significantly larger, so that the accessible area is big enough to be useful. An example of useful $C_{B \max}$ and $C_{B \min}$ can be seen in the case study presented in Sec. V.

Targeting the points that are enclosed in the area shown in Fig. 5 can be achieved by changing the ΔC_B and a_t within the achievable limits. Figures 6 and 7 show how these parameters need to change to target any point within the accessible area. The same values as in Fig. 5 have been used, except for the initial RAAN (which is why Fig. 6 is displaced westward). It is clear that having a positive ΔC_B

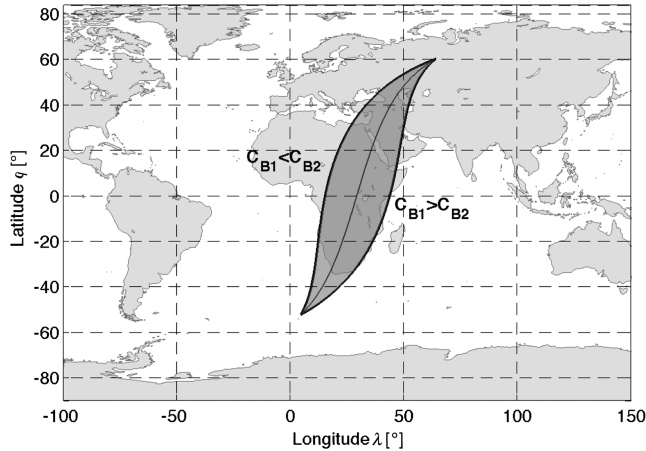


Fig. 5 Area that can be targeted by changing ΔC_B and the transition altitude a_t .

(so that $C_{B1} < C_{B2}$) moves the reentry point to the east and having a negative ΔC_B (so that $C_{B1} > C_{B2}$) moves the reentry point to the west. Then, if $\Delta C_B > 0$, increasing the transition altitude increases the argument of latitude of the reentry point, and if $\Delta C_B < 0$, increasing the transition altitude reduces the argument of latitude of the reentry point.

The longitude difference between the two exterior lines (maximum and minimum ΔC_B) at equal argument of latitude (equal latitude) can be used as a proxy for the amount of area that can be targeted. Figure 8 shows how this metric evolves when ΔC_B and the initial altitude h_0 are increased. The values used to produced the nominal curve (solid line) of this figure are as follows: $h_0 = 275$ km, $h_f = 100$ km, $C_{B \max} = 0.0225$ m²/kg, $C_{B \min} = 0.0215$ m²/kg, $i = 70$ deg, $H = 55$ km, $\rho_0 = 6.66 \times 10^{-12}$ kg/m³, and $a_{\rho_0} = 350$ km. The curve that shows the effect of an increased ΔC_B was generated by increasing the ΔC_B from 0.0005 to 0.0006 m²/kg. The curve that shows the effect of an increased initial altitude was generated by increasing h_0 to 278 km. As it could be expected, increasing the ΔC_B increases this longitude difference and therefore the area that can be targeted; also, increasing the initial altitude also increases the longitude differences and also retards the reentry argument of latitude (it takes longer to decay).

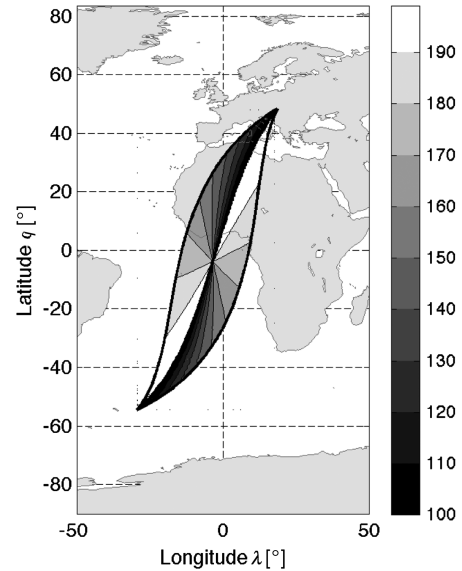


Fig. 7 Reentry point for different transition altitudes h_t .

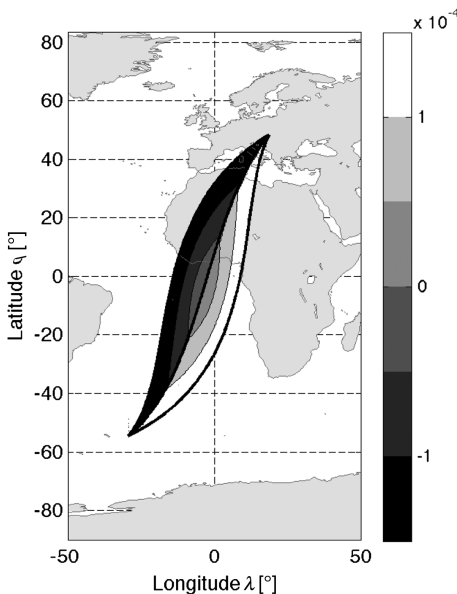


Fig. 6 Reentry point for different ΔC_B .

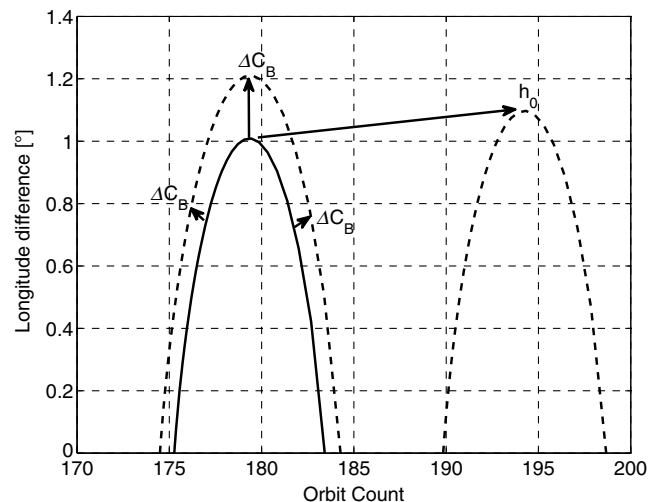


Fig. 8 Maximum longitude difference at equal argument of latitude. The dashed lines show the effect of increasing different parameters.

With this technique and a spacecraft that has the capability to change its ballistic coefficient, the atmospheric interface reentry location can be targeted. By increasing the initial altitude a_0 or increasing the range of ballistic coefficients available ΔC_B , the spacecraft will eventually achieve global coverage (the accessible latitude is obviously limited by the orbit's inclination). These minimum conditions to achieve global coverage are dependent on the atmospheric density, lower densities (low solar activity periods) increase the decay time, hence reducing the required initial altitude a_0 and range of ballistic coefficients available ΔC_B to achieve the global coverage.

These minimum conditions can be found by increasing a_0 and ΔC_B so that the accessible area covers the whole Earth. Figure 9 shows how the minimum required altitude to target any longitude at a particular latitude decreases as the ΔC_B range increases. The example shown assumes $C_{B\text{mean}} = 0.03 \text{ m}^2/\text{kg}$, an orbit inclination of 50 deg, a 0 deg target latitude, and the minimum altitude is computed in 0.1 km steps.

If, when this strategy is implemented, the minimum conditions to achieve global coverage are exceeded, it will often occur that when targeting a specific location there will be more than one solution. An example of the available solutions to target a specific location is provided in Fig. 10. Note that Fig. 10 shows multiple solutions (combinations of ΔC_B and a_t) when a single location is targeted. This

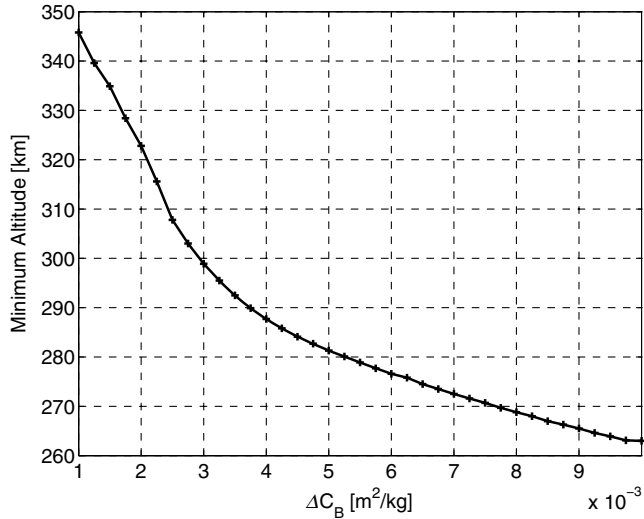


Fig. 9 Minimum required altitude to target any point with respect to ΔC_B .

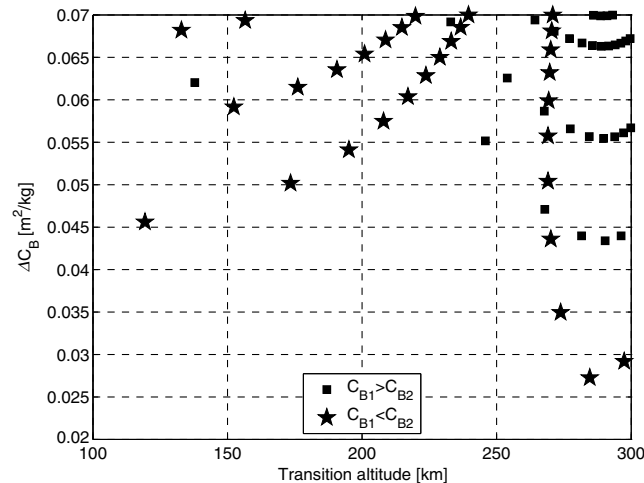


Fig. 10 Example of the solutions (using the case study from Sec. V) when exceeding the conditions for global coverage.

example uses the data provided in the case study presented in Sec. V. It is important to mention that the solutions have been computed with an initial altitude of 300 km (which is why the maximum transition altitude is also 300 km).

It also interesting to note that the solutions seem to define curves, although the solutions are discrete points. This tendency to define curves has not been explored in depth, although the shape of those curves seem to change for different scenarios.

In the case shown in Fig. 10, and ignoring any other constraints that the spacecraft may have, choosing the solution with the lower ΔC_B seems to be a good option because it is the solution that offers more margin of C_B to control the decay and cope with atmospheric uncertainties when implementing this option.

B. Numerical Approach

The behavior when the full dynamics are considered is more complex but very similar. The disadvantage is that the algorithms to identify the solution take much longer because, instead of evaluating analytical expressions, lengthy numerical propagations have to be performed. The analytical solutions could serve as a first guess for the numerical algorithms. The main challenge to have a good initial first guess is to adjust the exponential atmospheric model to match with more accurate and complex atmospheric models.

In the analytical approach, a simple exponential atmospheric model has been used. In the numerical approach, more realistic atmospheric models are required. For example, the NRMLSISE-00 [27], JB2008 [28] or DTM2013 [29] are recommended. Modeling the atmosphere is a complex task and an active field of research. Fortunately the International Organization for Standardization (ISO) provides some guidelines on how to model it [30].

In fact, the solutions are quite sensitive to the atmospheric conditions, and hence special care has to be taken when setting the parameters of the exponential model. If the exponential atmosphere density profile differs substantially from the atmospheric model used in the numerical approach, the solutions from the analytical and numerical approach will diverge. A way to solve this issue, and maintain good agreement between the analytical and numerical approach, is to break down the exponential atmosphere into altitude bands and apply different parameters (ρ_0 and H) within these bands. With this technique, a density profile that matches the density profile produced with atmospheric models used in numerical propagators can be generated.

Also, when propagating using the full dynamics of the system, the effects of the uncertainty of the parameters not present in the models has to be assessed. The uncertainty in the initial spacecraft position and velocity, in the solar radiation pressure, or in the gravity models will produce a reentry uncertainty footprint. This uncertainty footprint can be partially corrected during the decay by the control, but it already uses part of the controller range, which will no longer be available to control other expected errors or uncertainties that may arise during the decay (as changes in atmospheric density). Therefore, it is important to have accurate information of the spacecraft state vector and also of its properties. A case-by-case assessment has to be performed to assess the impact of these uncertainties.

It is also interesting to point out that, when extracting the solutions using a numerical approach, the simplifications in the dynamics and in the environmental models (atmosphere, gravity, third-body perturbations, and solar radiation pressure) can be dropped. The propagators used in the numerical approach can be as accurate as possible, and hence their solutions will include the effects of all these other forces and perturbations omitted in the analytical approach.

Because the intention is to use the analytical approach solutions as a first guess, there may be scenarios where it may be easier to add the perturbations in the numerical approach one at a time. For example, at the beginning, just add more gravity harmonics while maintaining all the other simplifications. The solution extracted in this case can be used as a first guess for a propagator that uses more gravity harmonics and also solar radiation pressure, for example. This process continues until all the perturbations are included. Using this step-by-step approach when adding the perturbations can be more time consuming

but ensures that the solutions change progressively (making it easier to converge).

IV. Navigation and Control

Once the nominal decay profile has been selected (a_i and ΔC_B), the spacecraft will have to control its decay to remain on target. Because this nominal decay will have been computed using simplified or inaccurate models, the spacecraft will have the tendency to deviate from the nominal decay path. The uncertainty in the atmospheric environment, mainly in density, is likely to be the main difference between the models used to compute the nominal decay and the real dynamics. Atmospheric models are not perfectly accurate [27,28,31] and the solar activity is difficult to forecast, hence making predictions of atmospheric densities difficult and inaccurate. To remain on target, with this atmospheric environment uncertainty, the ballistic coefficient can be adjusted to correct for the density uncertainty. In addition, the nominal decay can be updated regularly when more up-to-date atmospheric information becomes available.

Here, a simple control strategy is presented, although it is clearly not the only one that could be used and is not probably the most effective. This control strategy shows that the system is controllable. The computations required in this control strategy can be performed onboard the spacecraft, making the system autonomous, or can be performed on the ground and their results uplinked to the spacecraft. If conventional communication architectures are used (without relay satellites), the opportunities to downlink the information to the ground and uplink the results are limited to a few per day. An autonomous system may be more limited in terms of computing power but it can implement its results without delay, and hence the control can be adjusted more frequently. The simulation results from the control strategy presented here suggest that frequent updates are more important than a high accuracy, and hence the implementation of the controller onboard the spacecraft is favored.

Once the nominal decay trajectory has been computed, it is uploaded to the spacecraft. Then, to control this decay, the following process can be followed:

1) A Δt (time interval) is set. This time interval is set taking into account the current altitude and the aerodynamic capabilities of the spacecraft. Thus, Δt will change during the decay, as the altitude decreases, and will change from spacecraft to spacecraft, because they will have different aerodynamic properties.

2) The current state of the spacecraft is propagated forward p times the Δt time interval $p\Delta t$. The parameter p , is another parameter defined based on the altitude and the aerodynamic capabilities of the spacecraft.

3) The predicted future position is compared with the nominal decay position and velocity at that particular time.

4) The C_B at the n different Δt intervals are adjusted so that this error is minimized (this can be done using a simple least-square quadratic technique). The error normal to the orbit plane is not controlled because the change of the ballistic coefficient has very little effect on this direction.

5) The new C_B are implemented on the spacecraft.

6) The spacecraft orbits (decays) for a period of Δt with the new C_B , and then the process is repeated.

The propagation of the spacecraft state needs to be as precise as possible. During this step, all the previous assumptions to simplify the dynamics need to be dropped. Then, the inclusion of realistic gravity models (with high number of gravity harmonics), atmospheric models, solar radiation pressure, and third-body perturbations are desirable. Adding high-fidelity models will slow down the propagation, and it is possible the processing power and the time available for the propagation become the limiting factors. If this is the case, then more simplistic environmental models can be used (although the accuracy will decrease) and the control will lose effectiveness because it will try to correct the errors included in the propagation. A short Δt time period reduces the impact of the propagation errors.

This strategy controls the along-track and vertical differences in positions and velocity to make them track the nominal decay by

adjusting the spacecraft C_B . When the current state of the spacecraft is propagated by $p\Delta t$ and the propagation shows that the spacecraft has then reentered, then the strategy changes from matching the position and velocity in a future point to matching the time of reentry. The process is then the following:

1) A new Δt is set. Again, this time interval is set taking into account the current altitude and the aerodynamic capabilities of the spacecraft. Here, the rules to set the time interval may be different than the ones used before. These differences can make Δt experience a step change during the transition.

2) The current state of the spacecraft is propagated until reentry.

3) The predicted reentry time is compared with the nominal decay reentry time.

4) The C_B at the different Δt intervals until reentry are adjusted so that this error is minimized.

5) The new C_B are implemented on the spacecraft.

6) The spacecraft orbits (decays) for a period of Δt with the new C_B , and then the process is repeated until reentry.

This strategy only adjusts the ballistic coefficient to control the trajectory in the short term. Therefore, this strategy can only effectively correct the deviations in the orbit plane (both in position and velocity), but it has very limited capabilities to correct the deviations normal to the orbit plane. Fortunately, the main source of error comes from the uncertainty in the density that causes errors mainly in the along-track direction. Note that the uncertainty in the spacecraft ballistic coefficient behaves as the uncertainty in the density and can in fact be merged as a single uncertainty source (uncertainty in the drag force).

Also, in the absence of perturbations normal to the orbit plane, cross-track errors only occur when the decay deviates from the nominal one for long periods of time (same mechanism as the one used to obtain cross-track targeting capabilities). Therefore, maintaining a decay profile close to the nominal one (without bias) avoids cross-track deviations.

Because the atmospheric density decreases exponentially as the altitude increases, the Δt and p parameters have to be defined so that the uncertainty that dominates during the $p\Delta t$ is either the atmospheric or the ballistic coefficient uncertainty. As the altitude increases, other errors can become increasingly relevant, such as the error in the location and velocity of the spacecraft and the uncertainty in the solar radiation pressure. Trying to correct the solar radiation pressure (which can act in the normal plane direction) or trying to react over the state vector uncertainties (coming from GPS errors) can exhaust the control authority and mask out the deviations caused by the atmospheric and ballistic coefficient uncertainties, which are the ones that cause real errors in the reentry interface location in the long run. These others errors can effectively limit the applicability of this method at high altitudes, because these errors will dominate at high altitudes. Increasing the ΔC_B range would be required to be able to correct these other errors at lower altitudes by recomputing the nominal decay trajectory.

It is also worth mentioning that, if the deviations are large, the controller will saturate. In this case, the ballistic coefficient will be set to its maximum or minimum achievable value. The saturation is more likely to occur during the last stages of the decay, when the uncertainties in atmospheric density and ballistic coefficient have a bigger impact (hence requiring a larger control actuation). It is therefore important to size the ΔC_B range so that saturation happens as late as possible or that the impact of the saturation in the late stages of the decay is acceptable in terms of the reentry interface dispersion footprint. Nominal decay profiles that use nominal C_B closer to the $C_{B_{\text{mean}}}$ leave more of the ΔC_B range to the control, hence minimizing the saturation. So, when multiple nominal decay solutions are available, the one with nominal C_B closer to the $C_{B_{\text{mean}}}$ is recommended.

V. Case Study

The case of the Δ Dsat CubeSat is studied here to show how this method can be used in a real mission. The Δ Dsat spacecraft is a two unit CubeSat that is scheduled to fly as part of the QB50 network [32]. Its main scientific objectives are to study rarefied-gas aerodynamics

[33], to measure thermosphere winds, and demonstrate aerostability. To do so, it has four deployable panels that can rotate independently from one another, as seen in Fig. 11. This gives the CubeSat the ability to change its cross-sectional area and hence to change its ballistic coefficient from 0.02 to 0.16 m²/kg. This large range will allow ΔDsats to demonstrate the novel technique proposed here. One secondary objective will then be to make the spacecraft reenter over Cranfield University (United Kingdom), where the main ground station of the mission will be located. Targeting Cranfield would allow the Cranfield ground station, or other neighboring ground stations, to receive the CubeSat transmissions just before reentry (broadcasting its position) and hence assess if the technology demonstration has been successful or not. Targeting Cranfield does not pose any risk to property or population because the ΔDsats CubeSat will completely vaporize during reentry and no debris are expected to reach the ground.

Based on the latitude of Cranfield of 52°N, the 98 deg inclination of the orbit, and the aerodynamic capabilities of the CubeSat, the minimum required altitude for ΔDsats to ensure that it is able to target Cranfield regardless of the local time of the ascending node (which is still uncertain) is estimated to be between 240 and 250 km depending on the solar activity. Lower solar activity allows a lower starting altitude. Having such a low starting altitude for the reentry control allows the CubeSat to perform its other science experiments without interference at higher altitudes, because it will be deployed in a 380 km circular orbit.

To understand how all these different effects work together, a mission simulator (high-precision three-degree-of-freedom orbit propagator) has been developed to assess ΔDsats's expected accuracy. The simulator uses the NRLMSISE-00 model [27] to model the atmospheric density and the HWM93 model [34] to model the atmospheric wind. The simulator uses the EGM96 [35] gravity field model of the Earth. It also includes the gravity fields of the sun, the moon, and a realistic rotation of the Earth using the ITRF93 model [36] (celestial bodies ephemeris extracted using the SPICE toolkit from the Jet Propulsion Laboratory). The simulator also includes the perturbation of solar radiation pressure, assuming a reflectivity coefficient of $r = 0.9$.

Figure 10 shows an example of the solutions when Cranfield is targeted from an initial altitude of 300 km using ΔDsats. These solutions would change depending on the local time of the ascending node, which is still uncertain, and will also depend on the solar activity (because it drives the atmospheric density).

Figure 12 shows the expected reentry interface location dispersion 3σ from the target if the control method described in Sec. IV is applied and if an initial altitude of 250 km and a decay profile with $C_{B1} = 0.0715$ and $C_{B2} = 0.1209$ m²/kg is set. This case is then a realistic one because it simulates a typical decay profile with the segmented decay with two different ballistic coefficients equidistant to $C_{B\text{mean}} = 0.0962$ m²/kg.

To simulate the uncertainty of the atmospheric density and the spacecraft C_B , a Gaussian error of 20% 3σ has been introduced on the real C_B (biases of the atmospheric density are corrected by the navigation algorithm just by adjusting the mean C_B to cope with the

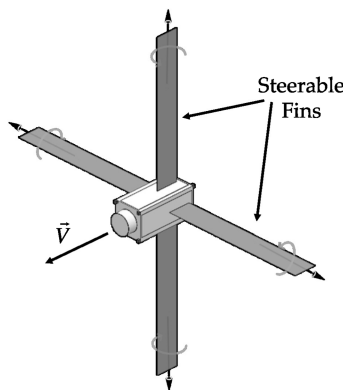


Fig. 11 Schematic representation of the ΔDsats 2U CubeSat.

bias). In addition, the HWM93 [34] wind model has been omitted in the control algorithms, but is included in the propagator to simulate the uncertainty of the winds. The knowledge of the spacecraft position and velocity contains a 4.5 m and 0.1 m/s 3σ error (based on the GPS unit to be flown) and a 15% uncertainty has been added to the solar radiation pressure forces. No uncertainty has been introduced in the gravity field model. Figure 12 shows the result of a 60 sample Monte Carlo simulation.

As can be seen in Fig. 12, the main dispersion occurs in the along-track direction with a much smaller dispersion in the cross-track direction. The estimated dispersion of the reentry interface location for ΔDsats is small enough so that, if Cranfield was targeted, the ground station from Cranfield, or other neighbor ground stations, could pick up the signals of the spacecraft emitted moments before it burns up. It is fair to say that the case presented here overestimates the control capability of the CubeSat, because some disturbances or delays have not been modeled. For example, it has been assumed that the onboard computer has enough computing power to handle orbit propagations with relatively high-fidelity models and that it does them instantly (no delays in applying the control ballistic coefficients). This will not be the case, the onboard propagator will probably use simpler models, and there will be delays in applying the output of the controller. These estimations will be refined before the launch of the mission.

Another interesting point is illustrated by observing the final C_B applied during the decay. Figure 13 shows the 3σ range of C_B applied

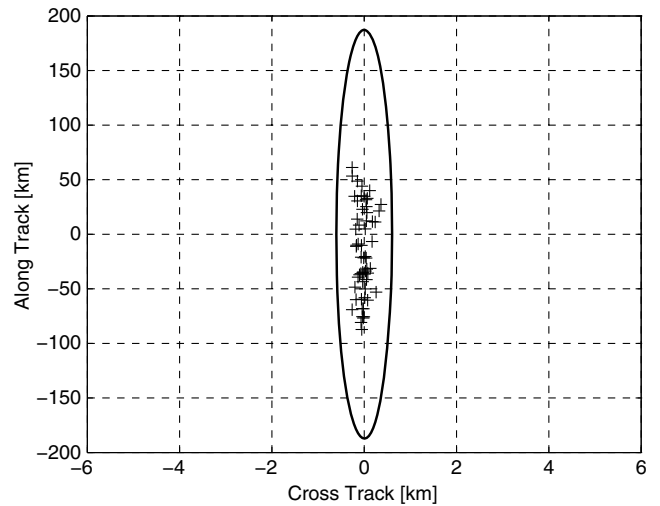


Fig. 12 Dispersion of the atmospheric interface reentry point from the target location.

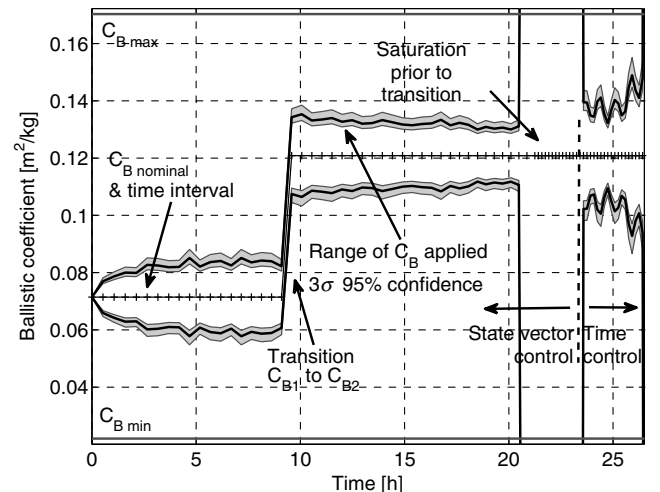


Fig. 13 C_B applied during the 60 sample Monte Carlo simulation.

in this 60 run Monte Carlo simulation. Note how the Δt time interval is shortened as the decay progresses. This keeps the C_B dispersion range constant and well below the limits of the spacecraft capabilities. Before the transition in strategy, the controller saturates in some of the simulated cases, but after the transition, the dispersion on the C_B is reduced, because the Δt time interval is reduced significantly (step reduction). As the spacecraft approaches the reentry interface, the dispersion in the applied C_B grows significantly again and it reaches the limits (hence saturating). To reduce this saturation, the Δt time interval could be reduced until the practical limit is reached.

VI. Potential Applications

The novel method presented here has mainly two major potential applications. The first one is in drag enhancing deorbiting devices. These devices increase the drag on a spacecraft after the end of the spacecraft operational life to speed up their decay, to reduce the risk of collision with other operational spacecraft or debris [37]. These devices are passive, and hence the location of the reentry is not controlled. On spacecraft that have components that will survive reentry, this can be a problem because they pose a risk to the population and to property. The method described in this paper could then be used to engineer a drag-enhancing deorbit device that could change the amount of drag it creates and hence control its reentry point. The reentry point could be selected to target remote areas such as the South Pacific. As these safe reentry areas are quite large, it requires a relatively low precision and hence a small ΔC_B range.

The second potential application is in passive small reentry capsules with inflatable heat shields [38]. In this case, a small reentry capsule could be crudely guided by this method using a similar device as the one used in ΔD_{sat} to reenter over a predefined area. The advantage of this method is that it is passive, and hence no propulsion is required. This allows for a cost and complexity reduction. Combining this method with an inflatable heat shield such as the one envisioned in [38], a complete targeted reentry system could be contained in a very small spacecraft (potentially down to a CubeSat size). This method is not very precise (refer to case study in Sec. V), and hence a large landing area will be expected. Therefore, part of the complexity is transferred to the search and recovery of the craft once on the ground.

It is obvious that including a device that can modulate the drag of a spacecraft and be used during the decay to target the atmospheric interface reentry can have a major impact on the spacecraft design and its operations. The case study shows a practical implementation of such a device (yet to be flown) and its scalability to bigger spacecraft is yet to be proven. It is clear then that, before the method presented here is used, it may need to be adapted to the specific mission requirements and spacecraft capabilities. It is possible to envision a system where the control of the ballistic coefficient is more limited than what has been assumed here (for example, limited range, larger ballistic coefficient steps for the control, or larger uncertainties). Also, the operations and design requirements that this method imposes may conflict with the requirements imposed by other mission objectives. This practical limitation may limit the applicability and performance of this method and may force it to adapt to the particular mission that will be using it.

VII. Conclusions

A novel method to control the reentry location of a spacecraft in a circular orbit by controlling its decay rate has been presented in this paper. Constructing the nominal decay is fairly simple when simplified dynamics are used. When more complex and realistic dynamics are considered, finding the nominal decay trajectory can be very computationally intensive. This can be a challenge when the nominal decay of a spacecraft needs to be recomputed between ground passes. Also, when considering full dynamics, the impact of the uncertainties in the spacecraft position and dynamic models needs to be taken into account. The case study has shown that the two-phase control algorithm has an acceptable performance for the example mission and for other potential applications. The range of ballistic

coefficient required is dependent on the mission profile and hence needs to be assessed on a per-case basis.

References

- [1] Leonard, C. L., Hollister, W. M., and Bergmann, E. V., "Orbital Formationkeeping with Differential Drag," *Journal of Guidance, Control, and Dynamics*, Vol. 12, No. 1, 1989, pp. 108–113. doi:10.2514/3.20374
- [2] Varma, S., and Kumar, K. D., "Multiple Satellite Formation Flying Using Differential Aerodynamic Drag," *Journal of Spacecraft and Rockets*, Vol. 49, No. 2, 2012, pp. 325–336. doi:10.2514/1.52395
- [3] Putnam, Z. R., and Braun, R. D., "Drag-Modulation Flight-Control System Options for Planetary Aerocapture," *Journal of Spacecraft and Rockets*, Vol. 51, No. 1, 2013, pp. 139–150. doi:10.2514/1.A32589
- [4] Vinh, N. X., Johannesen, J. R., Mease, K. D., and Hanson, J. M., "Explicit Guidance of Drag-Modulated Aeroassisted Transfer Between Elliptical Orbits," *Journal of Guidance, Control, and Dynamics*, Vol. 9, No. 3, 1986, pp. 274–280. doi:10.2514/3.20103
- [5] Miele, A., "1st John V. Breakwell Memorial Lecture: Recent Advances in the Optimization and Guidance of Aeroassisted Orbital Transfers," *Acta Astronautica*, Vol. 38, No. 10, 1996, pp. 747–768. doi:10.1016/S0094-5765(96)00076-8
- [6] Bevilacqua, R., and Romano, M., "Rendezvous Maneuvers of Multiple Spacecraft Using Differential Drag Under J2 Perturbation," *Journal of Guidance, Control, and Dynamics*, Vol. 31, No. 6, 2008, pp. 1595–1607. doi:10.2514/1.36362
- [7] Horsley, M., Nikolaev, S., and Pertica, A., "Small Satellite Rendezvous Using Differential Lift and Drag," *Journal of Guidance, Control, and Dynamics*, Vol. 36, No. 2, 2013, pp. 445–453. doi:10.2514/1.57327
- [8] Virgili, J., Roberts, P. C. E., Palmer, K., Hobbs, S., and Kingston, J., "Descending Sun-Synchronous Orbits with Aerodynamic Inclination Correction," *Journal of Guidance, Control, and Dynamics* (to be published). doi:10.2514/1.G000183
- [9] Pande, K., and Venkatachalam, R., "On Optimal Aerodynamic Attitude Control of Spacecraft," *Acta Astronautica*, Vol. 6, No. 11, 1979, pp. 1351–1359. doi:10.1016/0094-5765(79)90127-9
- [10] Psiaki, M. L., "Nanosatellite Attitude Stabilization Using Passive Aerodynamics and Active Magnetic Torquing," *Journal of Guidance, Control, and Dynamics*, Vol. 27, No. 3, 2004, pp. 347–355. doi:10.2514/1.1993
- [11] Ravindran, R., and Hughes, P. C., "Optimal Aerodynamic Attitude Stabilization of Near-Earth Satellites," *Journal of Spacecraft and Rockets*, Vol. 9, No. 7, 1972, pp. 499–506. doi:10.2514/3.61730
- [12] Gallais, P., *Atmospheric Re-Entry Vehicle Mechanics*, Springer, New York, 2007, pp. XXI–XXII.
- [13] Alemán, S., "Satellite Reentry Control via Surface Area Amplification," M.S. Thesis, U.S. Air Force Inst. of Technology, Wright–Patterson AFB, OH, 2009; also Technical Rept. ADA496111.
- [14] Patera, R., "Drag Modulation as a Means of Mitigating Casualty Risk for Random Reentry," AIAA Paper 2005-6228, 2005. doi:10.2514/6.2005-6228
- [15] Putnam, Z. R., and Braun, R. D., "Precision Landing at Mars Using Discrete-Event Drag Modulation," *Journal of Spacecraft and Rockets*, Vol. 51, No. 1, 2013, pp. 128–138. doi:10.2514/1.A32633
- [16] Phillips, R. L., "Use of Drag Modulation to Reduce Deceleration Loads During Atmospheric Entry," *ARS Journal*, Vol. 29, No. 6, 1959, pp. 414–422. doi:10.2514/8.4789
- [17] Hayes, J. E., "Satellite Landing Control System Using Drag Modulation," *ARS Journal*, Vol. 32, No. 5, 1962, pp. 722–730. doi:10.2514/8.6135
- [18] Rose, P. H., "Drag Modulation and Celestial Mechanics," *Advances in the Astronautical Sciences*, edited by Jacobs, H., Vol. 8, Plenum Press, New York, 1963, pp. 178–187.
- [19] Arthur, P. D., Baker, J. M., and Baxter, B. E., "Optimum Deboost Altitude for Specified Atmospheric Entry Angle," *AIAA Journal*, Vol. 1, No. 7, 1963, pp. 1663–1665. doi:10.2514/3.1880

- [20] Green, A. L., and Stern, G. S., "Optimum Deorbit Positioning for Minimum Impulse Reentry with Variable Reentry Conditions," *Journal of Astronautical Sciences*, Vol. 14, Jan. 1967, pp. 302–306.
- [21] Anandakrishnan, F. J. R. S. M., *Dynamics of Atmospheric Re-Entry*, AIAA Education Series, AIAA, Washington, D.C., 1993.
- [22] King-Hele, D. G., *Satellite Orbits in an Atmosphere: Theory and Application*, Blackie Academic and Professional, London, 1987, pp. 140–164.
- [23] Vallado, D., *Fundamentals of Astrodynamics and Applications*, 2nd ed., Microcosm Press, Hawthorne, CA, 2001, pp. 567–674.
- [24] Challinor, R., "Apparent Rotation of the Upper Atmosphere," *Planetary and Space Science*, Vol. 16, No. 5, 1968, pp. 557–566. doi:10.1016/0032-0633(68)90097-4
- [25] Drob, D. P., Emmert, J. T., Crowley, G., Picone, J. M., Shepherd, G. G., Skinner, W., Hays, P., Niecejewski, R. J., Larsen, M., She, C. Y., Meriwether, J. W., Hernandez, G., Jarvis, M. J., Sipler, D. P., Tepley, C. A., O'Brien, M. S., Bowman, J. R., Wu, Q., Murayama, Y., Kawamura, S., Reid, I. M., and Vincent, R. A., "Empirical Model of the Earth's Horizontal Wind Fields: HWM07," *Journal of Geophysical Research: Space Physics*, Vol. 113, No. A12, 2008, p. 304. doi:10.1029/2008JA013668.
- [26] Larson, W. J., and Wertz, J. R., *Space Mission Analysis and Design*, 3rd ed., Microcosm Press, Hawthorne, CA, 2005, pp. 131–155.
- [27] Picone, J. M., Hedin, A. E., Drob, D. P., and Aikin, A. C., "NRLMSISE-00 Empirical Model of the Atmosphere: Statistical Comparisons and Scientific Issues," *Journal of Geophysical Research: Space Physics*, Vol. 107, No. A12, 2002, Paper SIA 15.
- [28] Bowman, B. R., and Tobiska, W. K., "New Empirical Thermospheric Density Model JB2008 Using New Solar and Geomagnetic Indices," *AIAA/AAS Astrodynamics Specialist Conference*, AIAA Paper 2008-6438, 2008.
- [29] Bruinsma, S., "DTM2013 Evaluation Report," CNES, Toulouse, France, 2013.
- [30] "ISO 14222 Space Environment (Natural and Artificial). Earth Upper Atmosphere," International Organization for Standardization, Tech. Rept. 14222:2013, Geneva, 2013.
- [31] Pardini, C., Moe, K., and Anselmo, L., "Thermospheric Density Model Biases at the 23rd Sunspot Maximum," *Planetary and Space Science*, Vol. 67, No. 1, 2012, pp. 130–146. doi:10.1016/j.pss.2012.03.004
- [32] Muylaert, J.-M., Reinhard, R., Asma, C. O., Buchlin, J.-M., Rambaud, P., and Vetrano, M. R., "QB50, an International Network of 50 CubeSats for Multi-Point, In-Situ Measurements in the Lower Thermosphere and Re-Entry Research," *Atmospheric Science Conference*, Sept. 2009.
- [33] Virgili, J., and Roberts, P. C., "ΔDsats, a QB50 CubeSat Mission to Study Rarefied-Gas Drag Modelling," *Acta Astronautica*, Vol. 89, 2013, pp. 130–138.
- [34] Hedin, A. E., Fleming, E. L., Manson, A. H., Schmidlin, F. J., Avery, S. K., Clark, R. R., Franke, S. J., Fraser, G. J., Tsuda, T., Vial, F., and Vincent, R. A., "Empirical Wind Model for the Middle and Lower Atmosphere," *Journal of Atmospheric and Terrestrial Physics*, Vol. 58, No. 13, 1996, pp. 1421–1447. doi:10.1016/0021-9169(95)00122-0
- [35] Lemoine, F., "Geopotential Model EGM96," NASA Goddard Space Flight Center, Tech. Rept. TP-1998-206861, Greenbelt, MD, 1998.
- [36] Boucher, C., Altamimi, Z., and Duhem, L., "Results and Analysis of the ITRF93," International Earth Rotation and Reference Systems Service TN-18, 1994, pp. 1–313.
- [37] Hobbs, S., Kingston, J., Roberts, P., Juanes, C., Sewell, R., Snapir, B., Robinson, F., Virgili-Llop, J., Hobbs, J., and Patel, M., "De-Orbit Sail Design for TechDemoSat-1," *Proceedings 6th European Conference on Space Debris (ESA SP-723)*, ESOC, Darmstadt, Germany, April 2013.
- [38] Jason Andrews, K. B., and Watry, K., "Nanosat Deorbit and Recovery System to Enable New Missions," *Proceedings of the AIAA/USU Conference on Small Satellites, Mission Enabling Technologies II, SSC11-X-3*, AIAA, 2011, available online at <http://digitalcommons.usu.edu/smallsat/>.